Power efficiency of time-stretch imaging system by using parallel interleaving detection

Mengxuan Lv (吕孟轩)[1], Bo Dai (戴 博)[1,*], Songchao Yin (殷松超)[1], Dawei Zhang (张大伟)[1], and Xu Wang (王 旭)[2]

[1]*Engineering Research Center of Optical Instrument and System, the Ministry of Education, Shanghai Key Laboratory of Modern Optical System, University of Shanghai for Science and Technology, Shanghai 200093, China*

[2]*The Institute of Photonics and Quantum Sciences, School of Engineering and Physical Sciences, Heriot-Watt University, Edinburgh EH14 4AS, UK*

**Corresponding author: lioneldai2014@163.com*

Received May 25, 2016; accepted August 26, 2016; posted online September 30, 2016

A 38.88 MHz time-stretch line-scan imaging system with parallel interleaving detection is experimentally demonstrated. Since only half-chromatic dispersion is used to stretch optical pulses for wavelength-to-time mapping, the power efficiency is significantly improved by 6.5 dB. Furthermore, the theoretical analysis indicates that the power loss can be efficiently reduced for scan rates less than 100 MHz. In addition, a mathematical model for signal-to-noise evaluation is derived, including amplified spontaneous emission noise in the power compensation. Thanks to the improvement of the power efficiency by using parallel interleaving detection, the signal quality is enhanced.

OCIS codes: 110.2970, 320.7100, 100.0100.
doi: 10.3788/COL201614.101103.

Current high-end CCD or CMOS cameras are capable of capturing images at a frame rate of 100000 frames per second. However, the temporal resolution of a CCD or CMOS camera is not high enough to satisfy the requirements of a lot of scientific or industrial applications, where a temporal resolution of less than 1 μs is required. The temporal resolutions of CCD and CMOS cameras are mainly limited by the readout time for recording images from a two-dimensional pixel array. Some techniques, such as adding in-situ pixel level memory and using a cooling system, are put forward to reduce the readout time, but the improvement is at the expense of the spatial resolution and increasing the complexity and cost of the cameras. In addition, when CCD or CMOS cameras are used for ultrafast imaging, especially in the case of microscopic imaging, high-intensity illumination is required to make the cameras capture more photons so as to guarantee the sensitivity and signal-to-noise ratio (SNR). Nevertheless, high-intensity illumination may affect samples, e.g., damage to a cell illuminated by a focused beam on a micrometer scale.

Various ultrafast imaging techniques have been proposed to explore fast, dynamic unknowns[1,2]. Recently, a novel ultrafast imaging technique, serial time-encoded amplified microscopy (STEAM), was proposed[3–6]. In the STEAM technique, a broadband optical pulse is first spatially dispersed in free space for space-to-wavelength mapping to record the spatial pattern of an object into the spectrum. After image acquisition, the optical pulse is temporally dispersed in the time domain for wavelength-to-time mapping, and the dispersed pulse is then detected by using a single-pixel photodetector. Since photodetectors with more than 40 GHz bandwidths are commercially available nowadays, the image can be read out at an ultrafast speed. The STEAM technique's ability to acquire images at a frame rate of more than 6 MHz and at a line-scan rate of 1 GHz were demonstrated[3,7]. Besides, the STEAM technique actively captures images using spatially dispersed optical pulses. Therefore, it works in the dark field, and no high-intensity illumination is needed[8]. Furthermore, the STEAM technique can be developed into various modalities for different kinds of real-time measurements, including web inspection[9], vibration detection[4], three-dimensional profile measurements[10], optical coherence tomography (OCT)[11], displacement sensing[12], and real-time spectroscopy[13,14].

In the STEAM technique, the group velocity dispersion (GVD) for optical pulse stretching before detection has great influence over the spatial resolution. Usually, a high GVD is used to bring the imaging system into a spatial dispersion-limited operation in which the spatial resolution is independent of the GVD[15]. The number of pixels is proportional to the GVD as well. If the optical pulse is stretched significantly over the time domain, more samples can be collected by a digitizer with a limited sampling rate. Although a high GVD is beneficial to the spatial resolution and number of pixels, it results in a high insertion loss.

In this Letter, for the sake of energy efficiency, we propose to use parallel interleaving detection to read out image information. An imaging system with parallel interleaving detection is experimentally demonstrated, and the energy efficiency is investigated.

Figure 1 shows the time-stretch imaging system with the proposed parallel interleaving detection. A broadband

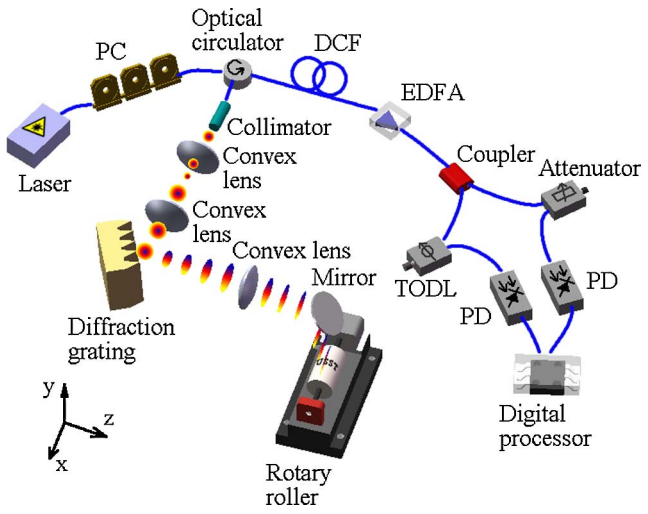

Fig. 1. Time-stretch imaging system with the parallel interleaving detection. PC: polarization controller. TODL: tunable optical delay line. PD: photodetector.

laser source is used to generate a sequence of short pulses. The short pulses are output to free space via an optical circulator and a collimator after polarization control. Then, the light passes a pair of biconvex lenses for beam size adjustment. The light after beam size expansion illuminates a diffraction grating and is spatially dispersed along the x-axis. The dispersed light is focused on the object by a biconvex lens. The spectrum of the light is modulated according to the reflectivity distribution of the object. After image acquisition, the light is reflected back and coupled into the optical fiber along the same optical path and output via Port 3 of the optical circulator. Next, a dispersion compensation fiber (DCF) is used for temporally stretching optical pulses. A chirped fiber Bragg grating can provide a high dispersion with low insertion loss[16], but a DCF is low cost and a specific GVD can be determined by using the proper length to avoid the overlapping of adjacent pulses. Due to the insertion loss of the DCF, an erbium-doped fiber amplifier (EDFA) is employed to compensate for the power loss. After signal amplification, the optical pulses are detected using parallel interleaving detection. The optical pulses are split into two optical paths. In the one optical path, an optical tunable delay line is used to split the optical pulses in the two paths that have a relative delay of $1/2R_S$, where R_S is the sampling rate of the digitizer. In the other optical path, an optical attenuator is used to balance the power in the two optical paths. Two photodetectors are used to detect the optical signals in the two paths separately. Finally, in the digitizer, the signals are sampled and interleaved together to recover the image.

The schematics of the conventional and proposed detection schemes are illustrated in Fig. 2. In the conventional scheme, the optical pulse is stretched as much as possible until it overlaps the adjacent optical pulses, e.g., over the time interval of $1/R$, where R is the repetition rate of the optical pulses. Then, the stretched optical pulse is directly

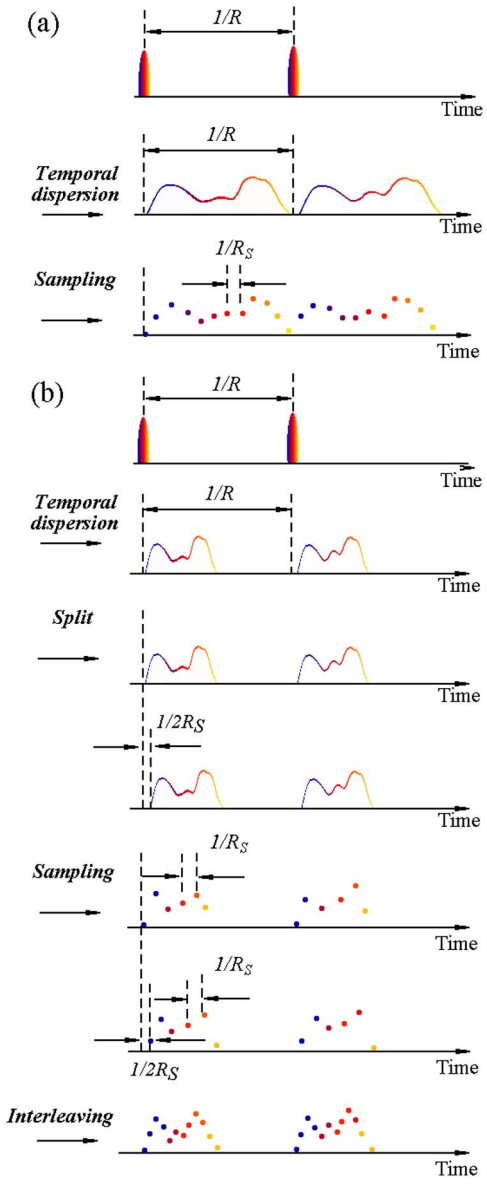

Fig. 2. Operation principle of (a) the conventional detection and (b) the parallel interleaving detection schemes in the time-stretch imaging system.

detected by a single-pixel photodetector and sampled by a digitizer of sampling rate of R_S. Since a high GVD for wavelength-to-time mapping is preferred to achieve a high spatial resolution and a large number of pixels, the loss for the time-stretching process is high.

In the proposed scheme, the optical pulse is only stretched with half the GVD as that in the conventional scheme. After that, the stretched pulse is split into two. The two optical pulses are detected by using two identical photodetectors in parallel. Then, the signals in the two channels are separately sampled at a sampling rate of R_S, and the sampling in the one channel leads that in the other channel by $1/2R_S$. Then, the samples from the two channels are interleaved to form a whole signal. Although only half the GVD is applied for pulse stretching and then half the samples are collected in the one channel,

the number of samples after interleaving is same as that in the conventional scheme at the same sampling rate. Besides, thanks to the parallel interleaving detection, the half-GVD leads to almost half the loss for the time stretch and the power efficiency is significantly improved.

In the experimental demonstration, a broadband femtosecond laser source is used. The repetition rate is externally modulated to 38.88 MHz, and the pulse width (FWHM) is about 90 fs. The center wavelength is at 1557 nm, and the −10 dB bandwidth is about 8 nm. In the image acquisition section, the beam size is expanded from 3.6 to 14.4 mm (the diameter where the intensity falls to $1/e^2$) by using a pair of biconvex lenses of 15 and 60 mm focal lengths. A diffraction grating of 600 lines/mm groove density is used to spatially disperse the light. The lens for focusing has a focal length of 150 mm. A non-reflective sheet coated with aluminum-sputtered film of a pattern of four letters, "USST," is used as a target. The height of the letters is about 800 μm. The microscopic image of the target is shown in Fig. 3(a). The target is fixed on a rotary roller with a diameter of 100 mm. The rotation speed is set to 300 rpm, corresponding to the approximately 1.5 m/s linear translation speed.

After image acquisition, a span of 12.1 km DCF is employed for the time stretch. The chromatic dispersion of the fiber is about 1.573 ns/nm, and the insertion loss is 10.8 dB. The photodetectors used in parallel interleaving detection have a bandwidth of 50 GHz. A 50 ps relative delay between the two channels is set, since the sampling rate of the digitizer is 10 GS/s. The insertion loss of the parallel interleaving detection is about 3.7 dB.

If the signal is detected by the conventional detection scheme, double chromatic dispersion is required for stretching the optical pulses and collecting as many samples as that in the demonstration, which implies that the insertion loss would be more than 21 dB. In the demonstration, the total insertion loss attributed to dispersion for the time stretch and parallel detection is only 14.5 dB, which a is more than 6.5 dB improvement.

Figure 3(b) shows the images obtained from both channels. The number of pixels is 125 × 760 (scan direction × rotation direction). Since the collected samples in the each channel are inadequate, the image size is small. Some abrasion of low reflectivity, which is highlighted in the red dashed circles, cannot be noticed. Figure 3(c) shows the recovered image after interleaving the signals in both channels. The pattern is recovered well. The number of pixels is 250 × 760 (scan direction × rotation direction). The details, including the defects and abrasion, can be clearly observed.

In the time-stretch imaging system, the scan rate limits the maximum chromatic dispersion used for wavelength-to-time mapping so as to avoid the overlapping of adjacent pulses. Besides that, the chromatic dispersion is closely related to the loss. Figure 4 shows the relation between the scan rate and the loss for the conventional system with sufficient time stretch and the system using parallel interleaving detection. In the analysis, the insertion loss of chromatic dispersion is 0.8 dB/km, and the chromatic dispersion is 130 ps/(nm km). The insertion loss of parallel interleaving detection is 3.7 dB. When the scan rate is low, it needs a high GVD to stretch the optical pulses, and the power loss of the chromatic dispersion for the time stretch is severe. The loss in the conventional system is almost twice that in the system using parallel interleaving detection due to the double dispersion. Nevertheless, if the scan rate is high, the influence of the power loss caused by chromatic dispersion becomes weak, and the 3 dB coupling for the optical pulse split is a dominant factor in the loss. Therefore, the parallel interleaving detection is suitable for time-stretch imaging systems with scan rates less than 100 MHz.

In addition, power amplification is necessary for the compensation of the power loss. However, the power amplification is accompanied by noise. The origin of the optical amplification noise is amplified spontaneous

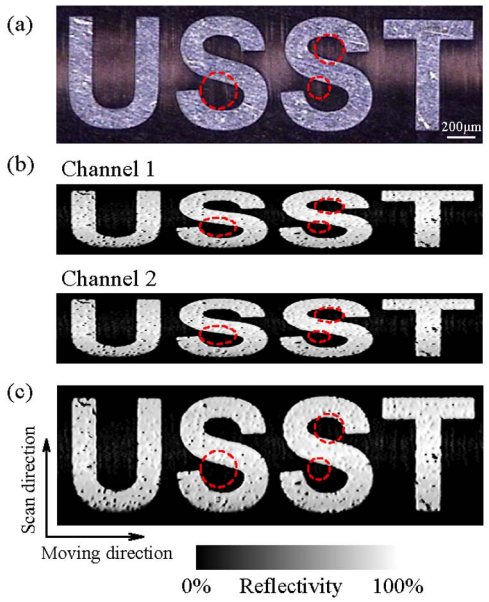

Fig. 3. (a) The bright-field microscopic image. (b) The images obtained from the two channels. (c) The recovered image after interleaving.

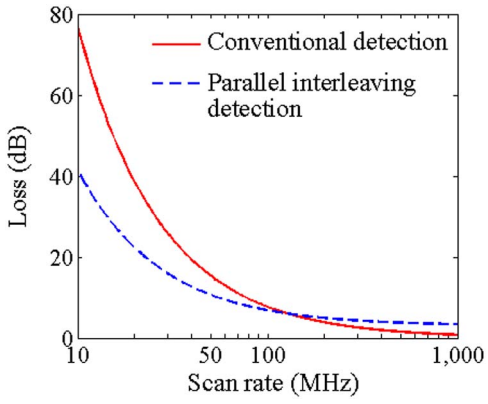

Fig. 4. Relation between power loss and scan rate.

emission (ASE). The power of the optical amplification noise can be expressed as

$$P_{\mathrm{Sp}} = 2S_{\mathrm{Sp}}\Delta v,$$

where S_{Sp} is the spectral density of spontaneous emission-induced noise, $S_{\mathrm{Sp}} = (G-1)n_{\mathrm{Sp}}\hbar v$, G is the gain of the power amplification, n_{Sp} is the spontaneous emission factor, $\hbar$ is the Planck constant, and v is the optical frequency. Δv is the optical bandwidth.

Considering the ASE induced by the optical amplification, the shot noise of the input light, the thermal noise of the photodetector, and the SNR can be written as

$$\mathrm{SNR} = \frac{P_{\mathrm{out}}^2}{\sigma_{\mathrm{Th}}^2 + \sigma_{\mathrm{Sh}}^2 + \sigma_{\mathrm{Beat}}^2} = \frac{P_{\mathrm{out}}^2}{f_{\mathrm{dig}}N_{\mathrm{th}} + 2ef_{\mathrm{dig}}(P_{\mathrm{out}} + \Re P_{\mathrm{Sp}}) + 4\Re P_{\mathrm{out}}S_{\mathrm{Sp}}f_{\mathrm{dig}}},$$

where P_{out} is the received power, and σ_{Th}, σ_{Sh}, and σ_{Beat} are the variances of the thermal noise, shot noise, and signal-ASE beat noise, respectively. f_{dig} is the bandwidth of the photodetector. N_{th} is the thermal noise spectral density. e is the electron charge. $\Re$ is the responsivity of the photodetection.

Figure 5 depicts the calculated SNR versus the received power with different gains of the amplification for power compensation. The parameters used for SNR calculation are listed in Table 1. In the calculation, it is found that the thermal noise (4×10^{-14}) and shot noise (1×10^{-12}–1×10^{-11}) are very low in contrast to signal-ASE beat noise (8×10^{-11}–8×10^{-10}) and can be neglected. The signal-ASE beat noise is proportional to the amplification gain. Since the system using parallel interleaving detection requires a relatively low amplification gain, the signal-ASE beat noise is low. Thus, the signal detected by the parallel interleaving detection scheme presents a better SNR.

In conclusion, a parallel interleaving detection scheme is proposed for a time-stretch imaging system to improve the power efficiency. In the experiment, a 38.88 MHz line-scan is demonstrated. With the assistance of parallel interleaving detection, the power loss is reduced by 6.5 dB, improving the power efficiency significantly. Besides that, the theoretical analysis of power efficiency indicates that using parallel interleaving detection is an efficient way to improve the power efficiency for a time-stretch imaging system with a frame rate less than 100 MHz. Furthermore, to evaluate the signal quality, a mathematical model for SNR calculation is derived. The theoretical result indicates that the signal-ASE beat noise is a dominant factor and a system using parallel interleaving detection can achieve a better SNR because a low amplification gain is required for power compensation.

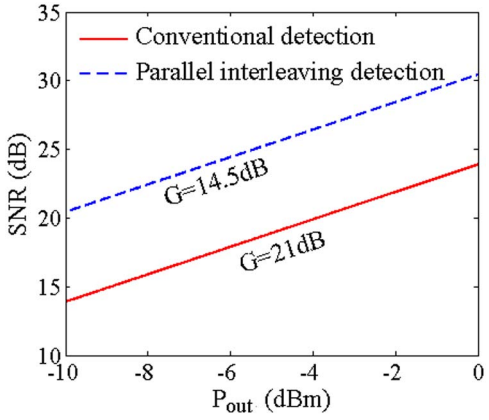

Fig. 5. SNR after amplification.

Table 1. Parameters and Constants Used in the SNR Calculation

Parameter	Value
f_{dig}	40 GHz
N_{th}	1 pA^2/Hz
$\Re$	0.8
n_{Sp}	2
V	192.68 THz
Δv	1 THz
G	14.5 dB for the parallel interleaving detection 21 dB for the conventional detection
$\hbar$	6.626×10^{-34} J · s
E	1.602×10^{-19} coulomb

This work was supported by the National Basic Research Program of China (No. 2015CB352001), the National Science Instrument Important Project (No. 2013YQ16043903), the Pujiang Project of Shanghai Science and Technology Commission (No. 14PJ1406900), and the Innovation Program of Shanghai Municipal Education Commission (No. 15ZZ071).

References

1. X. Jia, Y. Yuan, D. Yang, T. Jia, and Z. Sun, Chin. Opt. Lett. **12**, 113203 (2014).
2. D. Lu, X. Wang, S. Fan, J. He, Y. Zhou, and Y. Liu, Chin. Opt. Lett. **13**, 081102 (2015).
3. K. Goda, K. K. Tsia, and B. Jalali, Nature **458**, 1145 (2009).
4. K. Goda, A. Mahjoubfar, C. Wang, A. Fard, J. Adam, D. R. Gossett, A. Ayazi, E. Sollier, O. Malik, E. Chen, Y. Liu, R. Brown, N. Sarkhosh, D. D. Carlo, and B. Jalali, Sci. Rep. **2**, 445 (2012).
5. T. T. W. Wong, A. K. S. Lau, K. K. Y. Ho, M. Y. H. Tang, J. D. F. Robles, X. M. Wei, A. C. S. Chan, A. H. L. Tang, E. Y. Lam, K. K. Y. Wong, G. C. F. Chan, H. C. Shum, and K. K. Tsia, Sci. Rep. **4**, 3656 (2014).
6. B. Dai, R. Zhuo, S. Yin, M. Lv, R. Hong, Q. Wang, D. Zhang, and X. Wang, Opt. Lett. **41**, 882 (2016).
7. F. J. Xing, H. W. Chen, C. Lei, Z. L. Weng, M. H. Chen, S. G. Yang, and S. Z. Xie, Photon. Res. **2**, B31 (2014).

8. A. Yazaki, C. Kim, J. Chan, A. Mahjoubfar, K. Goda, M. Watanabe, and B. Jalali, Appl. Phys. Lett. **104**, 251106 (2014).
9. H. W. Chen, C. Wang, A. Yazaki, C. Kim, K. Goda, and B. Jalali, Appl. Opt. **52**, 4072 (2013).
10. B. Dai, D. Wang, Q. Wang, R. J. Hong, D. W. Zhang, and X. Wang, Photon. J. **7**, 6900509 (2015).
11. K. Goda, A. Fard, O. Malik, G. Fu, A. Quach, and B. Jalali, Opt. Express **20**, 19612 (2012).
12. K. Goda, K. K. Tsia, and B. Jalali, Appl. Phys. Lett. **93**, 131109 (2008).
13. J. Chou, Y. Han, and B. Jalali, Photon. Technol. Lett. **16**, 1140 (2004).
14. D. R. Soli, J. Chou, and B. Jalali, Nat. Photon. **2**, 48 (2008).
15. K. K. Tsia, K. Goda, D. Capewell, and B. Jalali, Opt. Express **18**, 10016 (2010).
16. T.-J. Ahn, Y. Park, and J. Azana, J. Sel. Top. Quantum Electron. **18**, 148 (2012).